RSC Advances

PAPER

View Article Online
View Journal | View Issue

Cite this: *RSC Adv.*, 2023, **13**, 18038

Transition metal dichalcogenide electrodes with interface engineering for high-performance hybrid supercapacitors

Muhammad Zahir Iqbal, *[ab] Misbah Shaheen, [b] Ahmad A. Ifseisi,[c] Sikandar Aftab,*[d] Zubair Ahmad,*[e] Sajid Hussain Siyal[f] and Muhammad Javaid Iqbal[g]

Received 14th May 2023
Accepted 2nd June 2023

DOI: 10.1039/d3ra03207h

rsc.li/rsc-advances

Transition metal dichalcogenides (TMDCs) have been explored in recent years to utilize in electronics due to their remarkable properties. This study reports the enhanced energy storage performance of tungsten disulfide (WS_2) by introducing the conductive interfacial layer of Ag between the substrate and active material (WS_2). The interfacial layers and WS_2 were deposited through a binder free method of magnetron sputtering and three different prepared samples (WS_2 and Ag-WS_2) were scrutinize *via* electrochemical measurements. A hybrid supercapacitor was fabricated using Ag-WS_2 and activated carbon (AC) since Ag-WS_2 was observed to be the most proficient of all three samples. The Ag-WS_2//AC devices have attained a specific capacity (Q_s) of 224 C g^{-1}, while delivering the maximum specific energy (E_s) and specific power (P_s) of 50 W h kg^{-1} and 4003 W kg^{-1}, respectively. The device was found to be stable enough as it retains 89% capacity and 97% coulombic efficiency after 1000 cycles. Additionally, the capacitive and diffusive currents were obtained through Dunn's model to observe the underlying charging phenomenon at each scan rate.

1 Introduction

Energy storage technology including batteries and supercapacitors are revolutionizing the industries in terms of their utilization from aerospace to daily use electronics.[1–4] Both energy storage devices (batteries and supercapacitors) are an inevitable part of current and next generation energy technology owing to their exciting features.[5–7] However, there are some challenges that need to be addressed regarding batteries and supercapacitors as both are not able to fulfil the demands by oneself due to exhibiting different charge storage mechanisms. The high power density (P_s) of supercapacitors is attributed to the electrostatically stored charges on the surface (electric double layer) or surface redox phenomenon (pseudocapacitors).[8] On the other hand, batteries deliver high energy density (E_s) by storing charges through bulk redox reactions.[9] To fix the aforementioned issues, batteries and capacitors can be conjoined in a single device to acquire the high E_s along with the high P_s.[10–13] The device comprises of both supercapacitor and battery grade electrode called a hybrid supercapacitor, being a proficient device that can certainly provide high E_s and P_s, high specific capacity (Q_s), coulombic efficiency and long-life cycling stability.[14,15]

Traditionally, carbonaceous materials such as activated carbon, graphene, reduce graphene oxide *etc.* are used for supercapacitors as they store charges on the surface providing good life stability.[16–22] Conversely, transition metals-based phosphates, sulfides, oxides *etc.* are adept in faradaically storing charges.[23–27] After graphene, revolution in energy technology has emanated due to layered transition metals dichalcogenides (TMDCs).[28,29] These 2D materials exist in MX_2 configuration (where M = metal ions; X = S, Se and/or Te).[30] TMDCs formation in XMX fashion allows them to possess some extraordinary physiochemical properties.[31] Different TMDCs have been reported for energy technology including MoS_2, WS_2, $MoSe_2$, WSe_2 and TiS_2 *etc.*, owing to their exciting properties such as high surface area, redox active sites, reactive structure *etc.*[32–34] These layer structured materials have observed to offer enhance electrochemical properties.[35] Thin sheets of TMDCs exhibit high storage capacity and energy density as they allow charges to adsorb on surface as well as to intercalate. The

[a]*Nanotechnology Research Laboratory, Faculty of Engineering Sciences, Ghulam Ishaq Khan Institute of Engineering Sciences and Technology, Topi 23640, Khyber Pakhtunkhwa, Pakistan. E-mail: zahir@giki.edu.pk*

[b]*ZENTECH Research Laboratory, Faculty of Engineering Sciences, Ghulam Ishaq Khan Institute of Engineering Sciences and Technology, Topi 23640, Khyber Pakhtunkhwa, Pakistan*

[c]*Department of Chemistry, College of Science, King Saud University, Riyadh 11451, Saudi Arabia*

[d]*Department of Intelligent Mechatronics Engineering, Sejong University, 209 Neungdong-ro, Gwangjin-gu, Seoul, 05006, South Korea. E-mail: aftab@sejong.ac.kr*

[e]*School of Chemical Engineering, Yeungnam University, 280 Daehak-ro, Gyeongsan, Gyeongbuk 38541, Republic of Korea. E-mail: zubair7157@yu.ac.kr*

[f]*Department of Metallurgy and Materials Engineering, Dawood University of Engineering and Technology, Karachi, 74800, Sindh, Pakistan*

[g]*Centre of Excellence in Solid State Physics, University of the Punjab, Pakistan*

decent properties of TMDCs make them potential candidate to utilize in energy technology.

Here, 2D tungsten disulfide (WS_2) was deposited on nickel foam through sputtering for energy storage application. Before deposition of WS_2, the interfacial layer of silver (Ag) was deposited to further enhance its electrochemical performance. The samples *i.e.*, WS_2 and Ag-WS_2 were prepared successfully. The fabricated electrodes were electrochemically tested in three electrode assembly to evaluate them for energy storage applications. Additionally, a real device was also fabricated composed of best suitable sample of TMDCs and activated carbon (AC) as hybrid supercapacitor.

2 Experimental

2.1 Deposition of interfacial layer and WS_2

Ollital multitarget RF-DC magnetron sputtering equipment was utilized for deposition for interfacial layer (Ag and Cu) and WS_2. The two different electrodes *i.e.*, WS_2, Ag-WS_2 were prepared through sputtering. First, the Ag particles were deposited on nickel foam (NF) substrates followed by a thin coating of WS_2 at a constant flow rate of 45 SCCM of argon gas. Substrate-target distance was maintained at 60 mm and thin films of WS_2 with thickness of 540 nm were successfully deposited at 300 V. The WS_2 sputtered NF substrates with and without interfacial layer of Ag were obtained.

2.2 Characterizations

X-ray diffraction (XRD), scanning electron microscopy (SEM), elemental dispersive X-ray (EDX) and Raman spectroscopy was executed for structural characterizations. Electrochemical measurements (cyclic voltammetry, Galvanostatic charge/discharge, electrochemical impedance spectroscopy) were done on GAMRY Reference 3000 potentiostat. All measurements were carried out in 1 M potassium hydroxide (KOH) electrolyte by making use of Hg/HgO as reference electrode and platinum wire as counter electrode. Potential window in three cell for WS_2 based samples was 0–0.7 V while for activated carbon −1 to 0 V potential window used. For two cell assembly, potential window was decided to be 0–1.6 V.

2.3 Fabrication process of hybrid supercapacitor

The nickel foam cuttings ($1 \times 1.5\ cm^2$) as substrate were utilized for deposition of interfacial layers and WS_2. Prior to the deposition, NF were ultrasonicated and cleaned with HCL, ethanol and DI water followed by the drying at 60 °C in vacuum oven. After deposition, all three working electrodes were separately tested in three cell assembly. Among all three samples, best performing electrode was chosen for hybrid supercapacitor device. The mass deposited on each electrode for three cell assembly was 4.00 mg however, to fabricate a device, charge balancing was done (eqn (1)) to gain the maximum output from the device.[36]

$$\frac{m_+}{m_-} = \frac{C_{s-} \times \Delta V_-}{C_{s+} \times \Delta V_+} \quad (1)$$

where, m denotes the masses, C_s present the capacitance and ΔV is the optimum potential window of positive (best sample) and negative electrode (activated carbon).

Also, the specific capacities were calculated in three as well as two cell assembly using cyclic voltammetry and galvanostatic charge/discharge (GCD) results through the eqn (2) and (3), respectively:[2]

$$Q_s = \frac{\int \mathrm{idV}}{mv} \quad (2)$$

$$Q_s = \frac{I \times t}{m} \quad (3)$$

where, in eqn (2), idV is the area possessed by CV curves, v denote the scan rate and m is the mass loaded on the electrode. In eqn (3), I/m is the current density and t is the time taken by sample to discharge.

The most important parameters *i.e.*, energy density (E_s) and power density (P_s) were calculated referring to the equations mentioned below:

$$E_s = \frac{Q_s \times \Delta V}{2 \times 3.6} \quad (4)$$

$$P_s = \frac{E_s \times 3600}{t} \quad (5)$$

where, Q_s denotes specific capacity, ΔV specifies potential window in eqn (4) whereas, E_s is the energy density in eqn (5) that was obtained through eqn (4).

The Dunn's model was also employed for the assessment of capacitive and diffusive currents by making use of equation below:

$$i = i_{\mathrm{capacitive}} + i_{\mathrm{diffusive}} \quad (6)$$

where,

$$i_{\mathrm{capacitive}} = k_1 v \quad (7)$$

$$i_{\mathrm{diffusive}} = k_2 v^{1/2} \quad (8)$$

3 Results and discussion

3.1 Structural and morphological study

For initial characterizations of WS_2, XRD was performed as depicted in Fig. 1a. The obtained peaks at 29°, 32.7°, 33.3°, 39°, 43.5°, 49.2°, 57.4°, 59° belong to the planes (004), (100), (101), (103), (006), (105), (110), (008), (116), respectively are in well agreement with the already reported studies and PDF # 08-0237.[37] Additionally, the sharp peaks with high intensity signify the high crystallinity and purity of WS_2. The Raman is also displayed in Fig. 1b agreed with the already reported Raman in previous studies. Two major bands of A_{1g} and E_{2g} are observed that are traditionally observed in WS_2.[38] Fig. 2a represent the SEM image of NF sputtered with pure WS_2. The porous structure can be clearly seen in the SEM. The EDX affirms the presence of

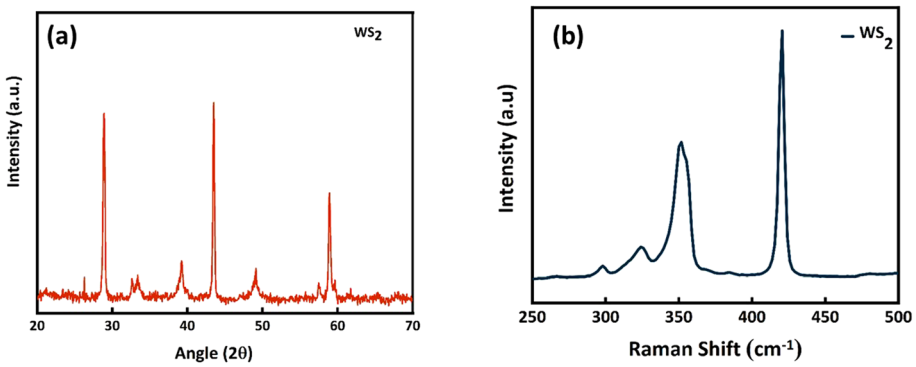

Fig. 1 (a) XRD and (b) Raman spectrum of WS_2.

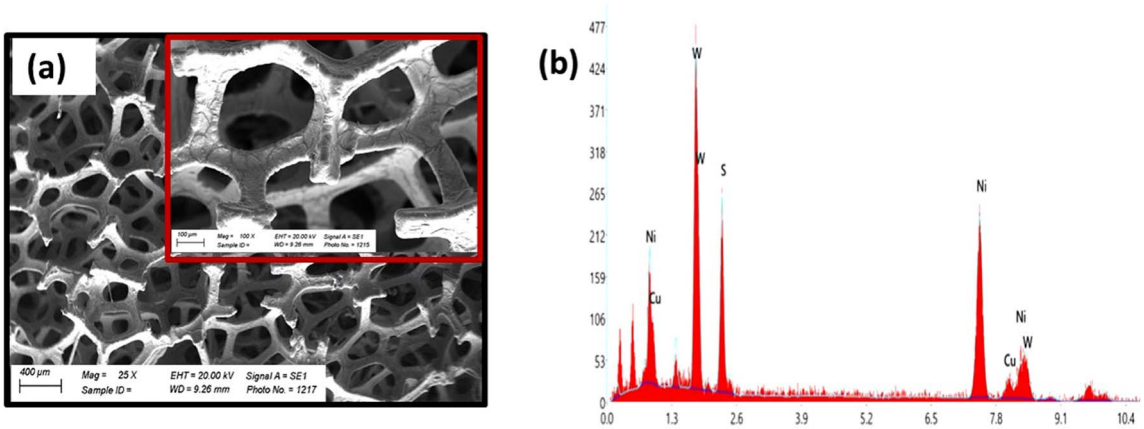

Fig. 2 (a) SEM and (b) EDX of WS_2.

tungsten and sulfur elements which is again presenting the evidence of WS_2 deposited on NF.

3.2 Electrochemical characterizations of electrodes in three cell assembly

The CV curves of WS_2 and Ag-WS_2 at various scan rates unveil the battery type behavior in three cell assembly (Fig. 3a and b). The obvious peaks are the evidence of redox reactions occurring due to the metal ion present in the active material. The +4 oxidation state of tungsten in WS_2 results in the two electron transfer that is clearly visible in the CV curves as two peaks are present in all samples between 0 and 0.4 V potential region. This type of faradaic dominant behavior or nearly battery grade nature is favorable condition for the fabrication of hybrid supercapacitors. However, to further enhance the conductivity and easy charge transfer, interfacial layers has been deposited to overcome the conductivity mismatch between the electrode (nickel foam) and active material (WS_2). The area under curves and currents got affected with the inclusion of Ag. The interfacial layer has enhanced the currents in comparison of the unchanged sample, and has proven to be more effective as highlighted in comparative CVs at 3 mV s^{-1} in Fig. 3c. Moreover, the shift in peaks is the confirmation of faradaic behavior of all samples and the retained shape of curves at all scan rates

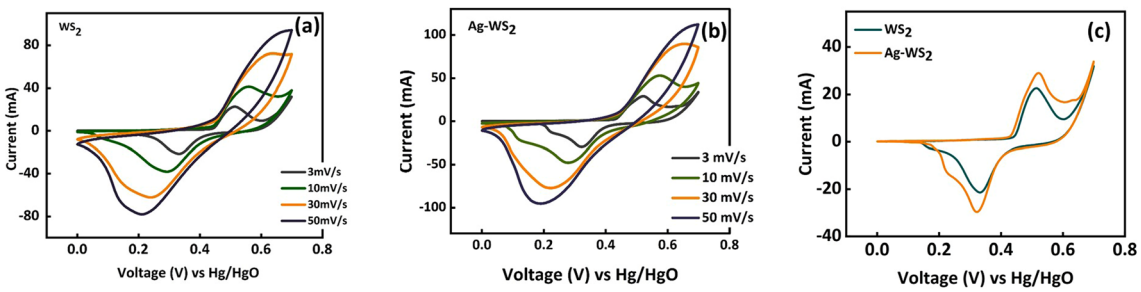

Fig. 3 Cyclic voltammograms of (a) WS_2 (b) Ag-WS_2, (c) comparison of CV curves of WS_2 and Ag-WS_2 at 3 mV s^{-1}.

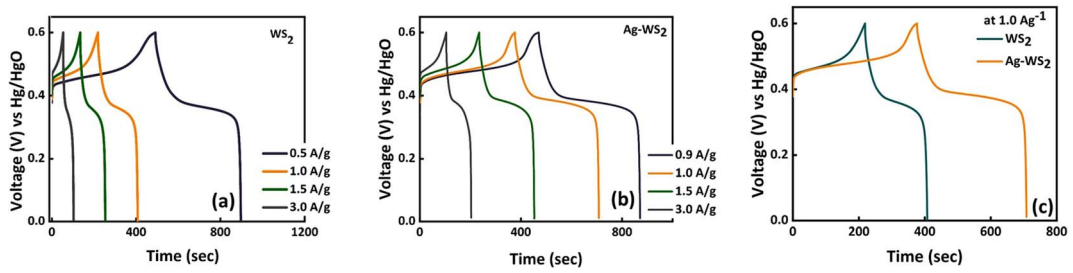

Fig. 4 Galvanostatic charge/discharge of (a) WS_2 (b) Ag-WS_2 (c) comparison of GCD curves of WS_2 and Ag-WS_2 at 1.0 A g^{-1}.

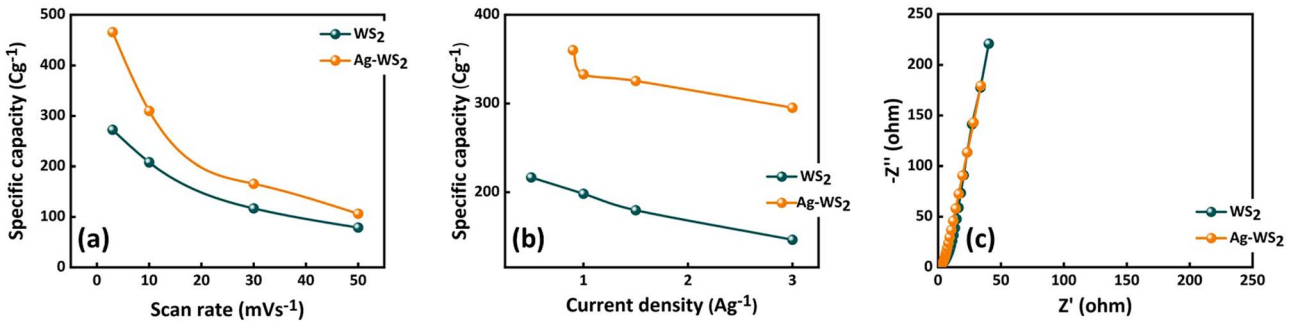

Fig. 5 (a) Specific capacity from CV, (b) specific capacity from GCD and (c) EIS of WS_2, and Ag-WS_2.

validates the stable structures of WS_2. The cyclic voltammograms are usually influenced by kinetically controlled processes. The peak shifts when scan rate increases because the elevated scan rates provide less time for ions to intercalate and/or perform redox reactions therefore, peaks slightly shift towards higher scan rate to successfully perform redox reactions.[20,21] For further understanding, GCD measurements were carried out to evaluate the samples for their charging and discharging behavior (Fig. 4a and b). The discernible humps in GCD of all samples replicates the peaks in corresponding CVs. These type of curvy GCDs suggests the battery type behavior that was already observed in CV measurements. Also, the GCD results show some IR drop representing a finite internal resistance exhibited by the system. Comparison of GCD results at 1.0 A g^{-1} in Fig. 4c are in support of CV results as the sample with Ag interfacial layer reveals the larger time *vs.* voltage curve indicating its best performance of all samples. The larger discharging time and slow voltage drop signifies the better capacity of Ag-WS_2 than WS_2. In addition, the specific capacities (Q_s) were calculated from CV and GCD at all scan rates and current densities for WS_2 and Ag-WS_2 by employing the eqn (2) and (3). The obtained Q_s are plotted in Fig. 5a and b and designate Ag-WS_2 a superior active material as it exhibits the Q_s of 466 C g^{-1} from CV and 361 C g^{-1} from GCD which is higher than WS_2 (CV: 267 C g^{-1}, GCD: 202 C g^{-1}). From the trend of specific capacity, the decline in capacity has been observed with increase in current density, the electrode or device reach to the given potential faster at higher current density than at lower current density which again limit the kinetics of the ions.[22] Another key parameter for energy storage devices is the conductivity of the system that was assessed from EIS measurements. The EIS graph plotted in Fig. 5c display no semicircle reveals the negligible charge transfer resistance (R_{ct}), whereas both the electrodes displayed the slight equivalent series resistance (ESR). The almost vertical straight line in low frequency region is another evidence of faradaic dominant nature of WS_2. Shorter length of linear line validates the fact that ions diffuse in Ag-WS_2 more easily than WS_2. Although, the samples have acceptable results, but the obtained results specify Ag-WS_2 as best performing sample in three cell assembly.

3.3 Electrochemical characterizations of electrodes in two cell assembly

As the Ag-WS_2 has been observed to be proficient enough to utilize for energy storage application so a hybrid supercapacitor was fabricated composed of Ag-WS_2 as positive (working) electrode and AC as negative (counter electrode) as schematically demonstrated in Fig. 6a. The quantity of active mass deposited on each electrode was obtained through mass balance equation (eqn (1)). The mass deposited was in ratio of 1 : 3 for Ag-WS_2 and AC, respectively. The three cell electrochemical results of AC and Ag-WS_2 are displayed in Fig. 6b and c for comparison and to understand the nature of AC. The rectangular curve of AC and Ag-WS_2 (Fig. 6b) directly points towards the capacitive behavior of AC and battery grade behavior of Ag-WS_2. Also, the GCDs of both electrodes (Fig. 6c) support the results obtained from CV. All the electrochemical results of the fabricated device (Ag-WS_2// AC) are showed in Fig. 7. The CV curves at several scan rates identify the hybrid nature of the device as the curves cover rectangular area along with the redox peaks (Fig. 7a). The both

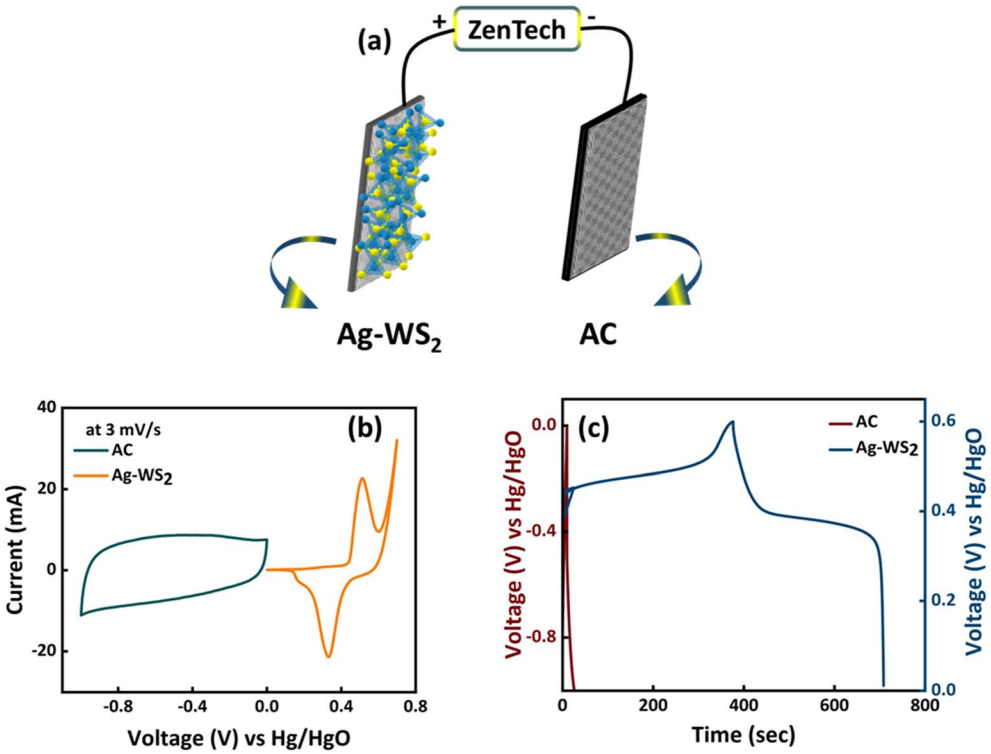

Fig. 6 (a) Schematic of asymmetric device Ag-WS_2//AC, (b) separate CVs of AC and Ag-WS_2 and (c) separate GCDs of AC and Ag-WS_2 in three cell assembly.

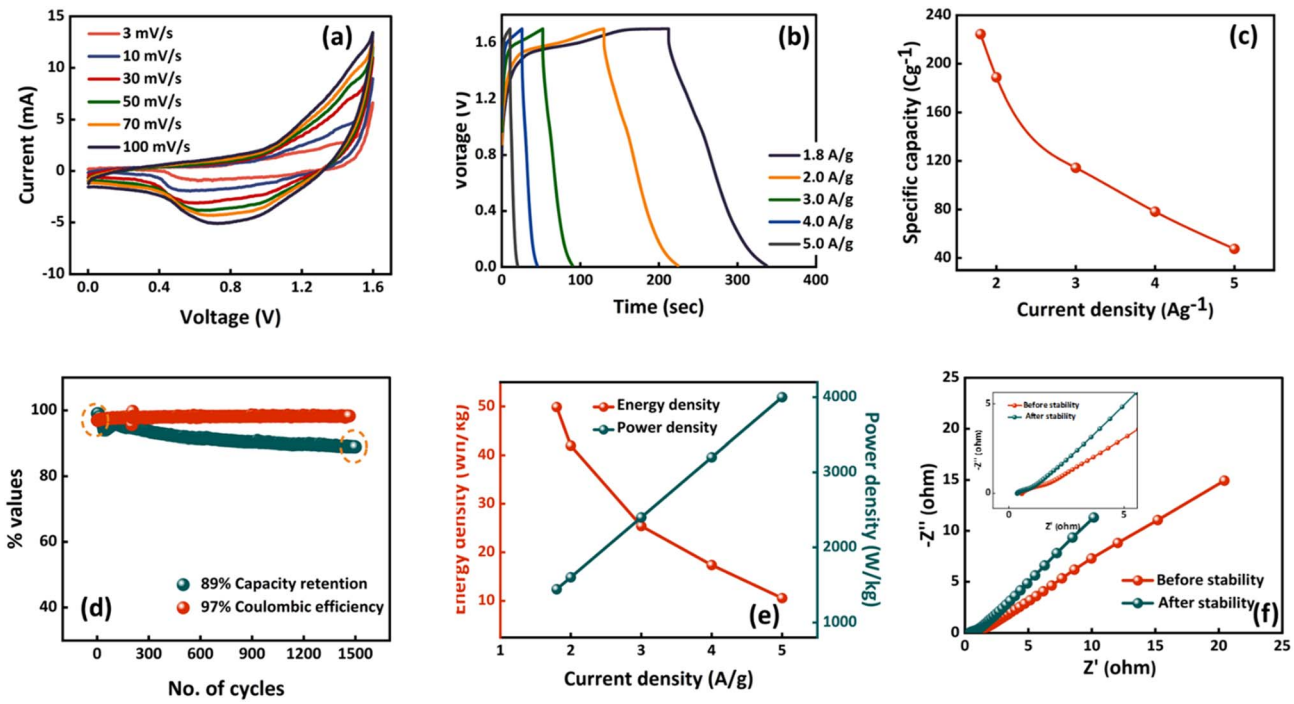

Fig. 7 (a) CV, (b) GCD, (c) specific capacity from GCD, (d) stability, (e) energy and power density and (f) EIS of Ag-WS_2//AC.

capacitive (AC) and battery grade (Ag-WS_2) electrodes take part in the final outcome to upraise the overall energy and power density. Similar behavior has been observed when GCD measurements were taken (Fig. 7b). The slight humps along with the linear region signifies the hybrid character of Ag-WS_2// AC device. The maximum specific capacity achieved was 224 C

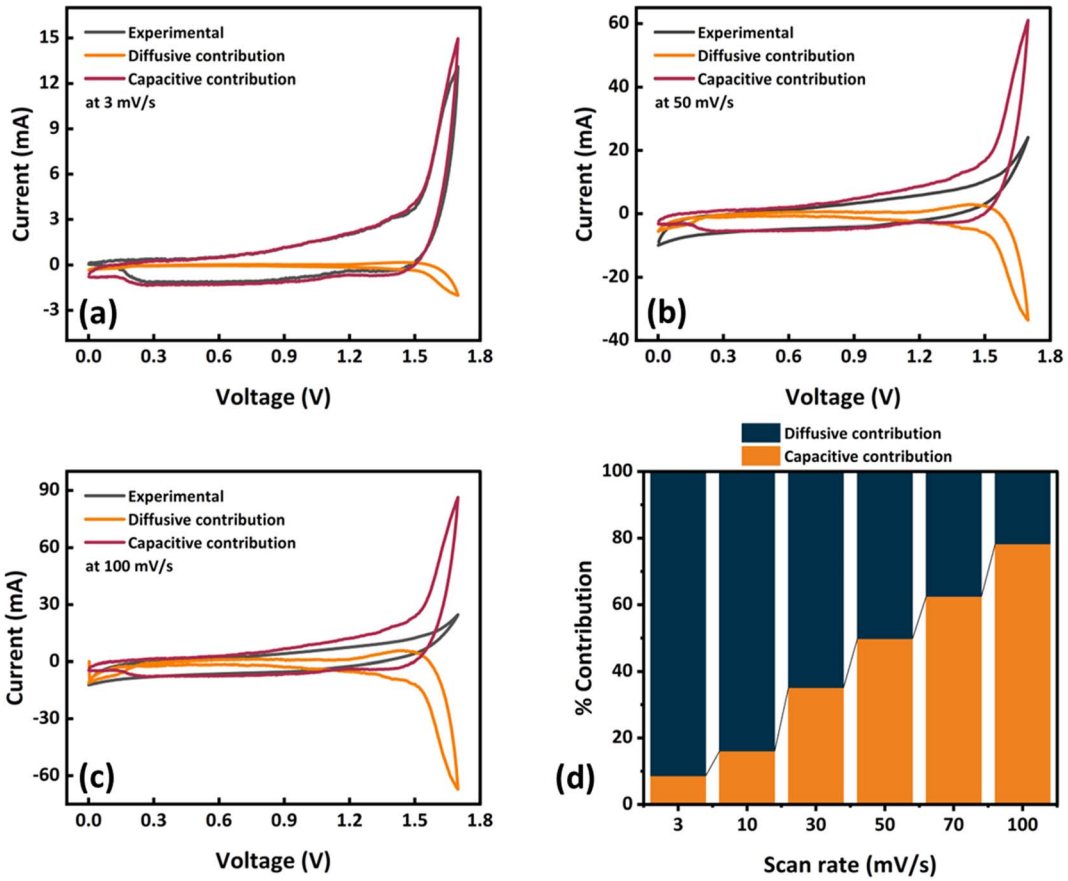

Fig. 8 $i_{capacitive}$ and $i_{diffusive}$ along with the experimental results at (a) 3, (b) 50, (c) 100 mV s^{-1}. (d) Percentage current contributions at scan rates ranges from 3 to 100 mV s^{-1}.

g^{-1} for the device and is plotted along with the series of Q_s at all current densities in Fig. 7c. The stability of the device was measured through the charging and discharging of device for 1000 times. It can be viewed in Fig. 6d that the device retains the capacity of 89% after 1000 cycles. Additionally, the 97% coulombic efficiency reflect the longer potential lifespan (Fig. 7d). The EIS outcomes before and after the stability test are demonstrated in Fig. 7e. The ESR and Warburg impedance has been slightly decreased after running 1000 GCD cycles as device becomes accustomed of hosting the incoming guest ions. Also, the indispensable parameters *i.e.*, E_s and P_s were calculated by making use of eqn (4) and (5). The maximum E_s and P_s effectuated for the device was 50 W h kg^{-1} and 4003 W kg^{-1}, respectively. All the obtained E_s and P_s values at different current densities are given in Fig. 7f. For further deep analysis, Dunn's model was utilized (eqn (6)) to scrutinize the interchanging behavior between capacitive ($i_{capacitive}$) and diffusive ($i_{diffusive}$) currents with change in scan rates. The $i_{capacitive}$ and $i_{diffusive}$ were extracted using Dunn's model and plotted in Fig. 8a–c for 3, 50 and 100 mV s^{-1}. The overall trend shows that the $i_{capacitive}$ becomes dominant as scan rate rises because of the fact that ions lose the capability of directly react with electrode due to the shorter time which ultimately discourage the faradaic behavior. The percentage of $i_{capacitive}$ and $i_{diffusive}$ is plotted as bar chart against the scan rates in Fig. 8d showing the faradaic dominant behavior at low scan rates while the ascending trend for capacitive current was noticed. The overall results of hybrid supercapacitor stipulate WS_2 as an efficient electrode material for energy storage applications.

4 Conclusion

In recent times, the exploration of new electrode materials for energy storage applications is in great demand. TMDCs being incredible series of 2D materials exhibit amazing structural, electrical and electrochemical properties. Owing to them, a hybrid supercapacitor was fabricated using WS_2 however, with some modifications. Interfacial layers of Ag and Cu were deposited separately prior to the deposition of WS_2 and tested for their energy storage performance. Obtaining Ag-WS_2 as best performing electrode, its hybrid supercapacitor device was fabricated with activated carbon which revealed the significant Q_s (224 C g^{-1}) along with the substantial E_s (50 W h kg^{-1}), P_s (4003 W kg^{-1}) and stability of 89% after 1000 cycles. Ag layer was proved to improve the electron transfer process by minimizing the conductivity mismatch between the electrode and WS_2. This work gives a direction towards the enhancement of energy storage capabilities of the electrode materials.

Conflicts of interest

There are no conflicts to declare.

Acknowledgements

The authors are grateful to the Researchers Supporting Project number (RSPD2023R669), King Saud University, Riyadh, Saudi Arabia, for the financial support.

References

1 E. Karden, S. Ploumen, B. Fricke, T. Miller and K. Snyder, *J. Power Sources*, 2007, **168**, 2–11.
2 Y. Shao, M. F. El-Kady, J. Sun, Y. Li, Q. Zhang, M. Zhu, H. Wang, B. Dunn and R. B. Kaner, *Chem. Rev.*, 2018, **118**, 9233–9280.
3 J. Zhao and A. F. Burke, *J. Energy Chem.*, 2021, **59**, 276–291.
4 M. Wakihara, *Mater. Sci. Eng., R*, 2001, **33**, 109–134.
5 B. Jin, J.-U. Kim and H.-B. Gu, *J. Power Sources*, 2003, **117**, 148–152.
6 H. Kim, W. Choi, J. Yoon, J. H. Um, W. Lee, J. Kim, J. Cabana and W.-S. Yoon, *Chem. Rev.*, 2020, **120**, 6934–6976.
7 X.-y. Luo, Y. Chen and Y. Mo, *New Carbon Mater.*, 2021, **36**, 49–68.
8 M. Salanne, B. Rotenberg, K. Naoi, K. Kaneko, P. L. Taberna, C. P. Grey, B. Dunn and P. Simon, *Nat. Energy*, 2016, **1**, 16070.
9 D. Saurel, B. Orayech, B. Xiao, D. Carriazo, X. Li and T. Rojo, *Adv. Energy Mater.*, 2018, **8**, 1703268.
10 D. P. Chatterjee and A. K. Nandi, *J. Mater. Chem. A*, 2021, **9**, 15880–15918.
11 N. R. Chodankar, H. D. Pham, A. K. Nanjundan, J. F. S. Fernando, K. Jayaramulu, D. Golberg, Y.-K. Han and D. P. Dubal, *Small*, 2020, **16**, 2002806.
12 M. F. El-Kady, M. Ihns, M. Li, J. Y. Hwang, M. F. Mousavi, L. Chaney, A. T. Lech and R. B. Kaner, *Proc. Natl. Acad. Sci.*, 2015, **112**, 4233–4238.
13 M. Z. Iqbal and J. Khan, *Electrochim. Acta*, 2021, **368**, 137529.
14 X. Han, B. Wang, C. Yang, G. Meng, R. Zhao, Q. Hu, O. Triana, M. Iqbal, Y. Li, A. Han and J. Liu, *ACS Appl. Energy Mater.*, 2019, **2**, 2072–2079.
15 S. S. Patil, T. S. Bhat, A. M. Teli, S. A. Beknalkar, S. B. Dhavale, M. M. Faras, M. M. Karanjkar and P. S. Patil, *Eng. Sci.*, 2020, **12**, 38–51.
16 Y. Wang, L. Zhang, H. Hou, W. Xu, G. Duan, S. He, K. Liu and S. Jiang, *J. Mater. Sci.*, 2021, **56**, 173–200.
17 L. L. Zhang and X. S. Zhao, *Chem. Soc. Rev.*, 2009, **38**, 2520–2531.
18 S. Bose, T. Kuila, A. K. Mishra, R. Rajasekar, N. H. Kim and J. H. Lee, *J. Mater. Chem.*, 2012, **22**, 767–784.
19 Y.-r. Zhao, C.-c. Liu, Q.-q. Lu, O. Ahmad, X.-j. Pan and M. Daria, *New Carbon Mater.*, 2022, **37**, 875–897.
20 K. Yousefipour, R. Sarraf-Mamoory and S. Mollayousefi, *RSC Adv.*, 2022, **12**, 27868–27876.
21 K. Yousefipour, R. Sarraf-Mamoory and A. Yourdkhani, *Colloids Surf., A*, 2022, **647**, 129066.
22 K. Yousefipour, R. Sarraf-Mamoory and A. Yourdkhani, *Surf. Interfaces*, 2022, **29**, 101638.
23 X. Li, X. Xiao, Q. Li, J. Wei, H. Xue and H. Pang, *Inorg. Chem. Front.*, 2018, **5**, 11–28.
24 M. F. Iqbal, M. N. Ashiq and M. Zhang, *Energy Technol.*, 2021, **9**, 2000987.
25 C. An, Y. Zhang, H. Guo and Y. Wang, *Nanoscale Adv.*, 2019, **1**, 4644–4658.
26 Z. Huang, R. Zhang, S. Zhang, P. Li, C. Li and C. Zhi, *Mater. Futures*, 2022, **1**, 022101.
27 K. Yousefipour, R. Sarraf-Mamoory and A. Chaychi Maleki, *J. Energy Storage*, 2023, **59**, 106438.
28 R. N. A. R. Seman, M. A. Azam and M. H. Ani, *Nanotechnology*, 2018, **29**, 502001.
29 J. Cherusseri, N. Choudhary, K. Sambath Kumar, Y. Jung and J. Thomas, *Nanoscale Horiz.*, 2019, **4**, 840–858.
30 A. V. Kolobov and J. Tominaga, in *Two-Dimensional Transition-Metal Dichalcogenides*, ed. A. V. Kolobov and J. Tominaga, Springer International Publishing, Cham, 2016, pp. 29–77, DOI: 10.1007/978-3-319-31450-1_3.
31 X. Wu, H. Zhang, J. Zhang and X. W. Lou, *Adv. Mater.*, 2021, **33**, 2008376.
32 Y. Liu, D. Zhao, H. Liu, A. Umar and X. Wu, *Chin. Chem. Lett.*, 2019, **30**, 1105–1110.
33 F. Yang, H. Guo, J. Zhang, N. Wu, M. Yang, Y. Chen, T. Zhang, L. Sun and W. Yang, *J. Energy Storage*, 2022, **54**, 105234.
34 M. Habib, A. Khalil, Z. Muhammad, R. Khan, C. Wang, Z. u. Rehman, H. T. Masood, W. Xu, H. Liu, W. Gan, C. Wu, H. Chen and L. Song, *Electrochim. Acta*, 2017, **258**, 71–79.
35 R. A. W. Dryfe, *Curr. Opin. Electrochem.*, 2019, **13**, 119–124.
36 D. M. Sayed, M. M. Taha, L. G. Ghanem, M. S. El-Deab and N. K. Allam, *J. Power Sources*, 2020, **480**, 229152.
37 Y. Lv, F. Huang, L. Zhang, J. Weng, S. Zhao and Z. Ji, *Coatings*, 2018, **8**, 205.
38 K. H. Shin, M.-K. Seo, S. Pak, A.-R. Jang and J. I. Sohn, *Nanomaterials*, 2022, **12**, 1393.